PROCEEDINGS OF SCIENCE

Calculating $K \to \gamma\gamma$ using lattice QCD

Yidi Zhao[a] **and Norman H. Christ**[a,*]

[a] *Department of Physics, Columbia University,*
538 W 120th Street, New York, USA

E-mail: yz3210@columbia.edu, nhc@phys.columbia.edu

Determining the standard model prediction for the decay amplitude of a long-lived neutral kaon into two photons is an important step toward the goal of calculating the two-photon contribution to $K_L \to \mu^+\mu^-$ decay. In this talk we describe a computational strategy to determine this decay amplitude using lattice QCD. While the lattice QCD calculation is carried out in finite volume, the emitted photons are treated in infinite volume and the resulting finite-volume errors decrease exponentially in the linear size of the lattice volume. Only the CP-conserving contribution to the decay is computed and we must subtract unphysical contamination resulting from single pion and eta intermediate states which grows exponentially (or falls slowly) as the time separation between the initial and final lattice operators is increased. First results from a calculation on a $24^3 \times 64$ lattice volume with $1/a = 1$ GeV and physical quark masses are presented.

The 38th International Symposium on Lattice Field Theory, LATTICE2021 26th-30th July, 2021
Zoom/Gather@Massachusetts Institute of Technology

*Speaker

PoS(LATTICE2021)451

1. Introduction

The rare decay $K_K \to \mu^+\mu^-$ is a flavor-changing neutral-current process which occurs at second-order in the weak interaction and involves the exchange of a W and a W or a Z boson. This is a short-distance-dominated process with an accurately measured branching ratio of $6.84(0.11) \times 10^{-9}$ [1] which can also be reliably calculated in perturbation theory. It should serve as an important test of the standard model at one-loop. However, such a test is not possible because the third-order electroweak process which involves a single W boson and two-photon exchange shown in Fig. 1(a) gives a contribution to this decay which is of a similar size and presents a background which is not adequately known.

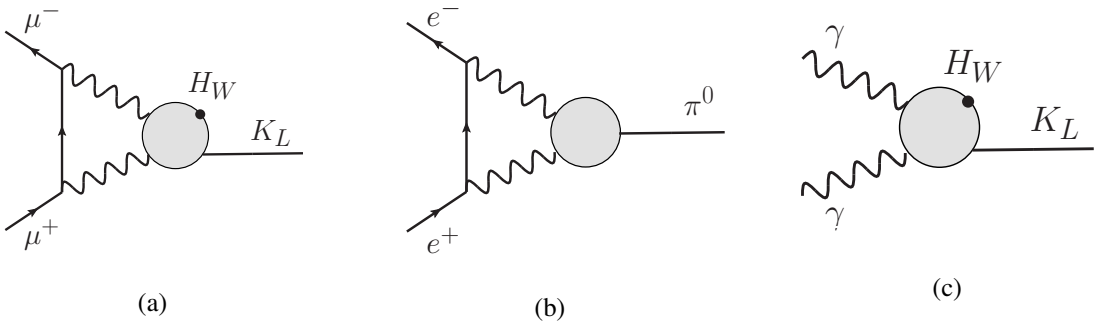

Figure 1: Schematic representations of the three processes discussed in this paper. (a) The two-photon contribution to the decay $K_L \to \mu^+\mu^-$ whose lattice QCD calculation is the ultimate target of this project. (b) The simpler decay $\pi^0 \to e^+e^-$ which involves some of the complications of $K_L \to \mu^+\mu^-$ and (c) The decay $K_L \to \gamma\gamma$ which is the calculation reported here.

While a traditional lattice QCD calculation of this two-photon-exchange contribution to $K_L \to \mu^+\mu^-$ decay involves an eight-point function and would appear to be impractical, advances introduced in the calculation of the hadronic light-by-light contribution to the anomalous magnetic moment of the muon [2, 3], a six-point function which may offer strategies that can be applied here.

The first step in this direction was a calculation of the simpler $\pi^0 \to e^+e^-$ decay [4, 5], shown in Fig. 1(b). Here no weak interaction vertex is involved and, more important, there is no intermediate hadronic state with a mass smaller than that of the initial pion. The presence of hadronic states with mass smaller than that of the decaying state introduces unphysical contributions into a Euclidean-space calculation which must be removed if the decay process of interest is to be studied. However, it was shown that with an appropriate choice of integration contour for the loop containing the two photon and electron propagators, the $\pi^0 \to e^+e^-$ decay amplitude could be expressed as the integral of the product of a known complex function coming from the two photon and electron propagators multiplied by a Euclidean amplitude given by the matrix element of product of two electromagnetic currently evaluated between the π^0 state and the vacuum – a matrix element that can be computed using lattice methods.

In this paper we consider other challenges posed by the $K_L \to \mu^+\mu^-$ calculation: the presence of the extra H_W vertex and possible intermediate states with energy less than M_K by beginning a calculation of the process $K_L \to \gamma\gamma$, shown in Fig. 1(c). We will neglect CP violation so the final

two-photon state will be parity odd, similar to the final two photons in the decay $\pi^0 \to \gamma\gamma$ and the decay amplitude can be described by a single amplitude $F_{K_L\gamma\gamma}$:

$$\langle\gamma(k_1,\varepsilon_1)\gamma(k_2,\varepsilon_2)|\mathcal{H}_W(0)|K_L(k)\rangle = c\epsilon^{\mu\nu\rho\delta}(k_1)_\mu(k_2)_\nu(\varepsilon_1)_\rho(\varepsilon_2)_\delta F_{K_L\gamma\gamma} \tag{1}$$

where $\mathcal{H}_W(x)$ is the effective weak Hamiltonian density. The normalization constant c is defined so that the $K_L \to \gamma\gamma$ decay rate is given by:

$$\Gamma(K_L \to \gamma\gamma) = \frac{\pi}{4}M_K^3\left[\alpha\frac{G_F}{\sqrt{2}}V_{us}V_{ud}F_{K_L\gamma\gamma}\right]^2, \tag{2}$$

where V_{us} and V_{ud} are the usual CKM matrix elements, α the fine structure constant and G_F the Fermi constant. The experimental value for $F_{K_L\gamma\gamma}$ determined from the decay rate is $F_{K_L\gamma\gamma} = 0.02047(9)$ GeV.

2. Lattice formulation

In order to compute the amplitude $F_{K_L\gamma\gamma}$ in Eq. (1) using lattice QCD we must change from Minkowski to Euclidean time dependence and perform a calculation in a finite volume. We begin with a standard expression for the decay amplitude in which the integrals over the time coordinates of the two electromagnetic currents have been rotated to Euclidean time:

$$\begin{aligned}\mathcal{A}(\vec{k},\varepsilon_1,\varepsilon_2) &= \int d^3u\, d^3v e^{-i(\vec{u}-\vec{v})\cdot\vec{k}}\int_{-\infty}^{+\infty}dv_0\int_{v_0}^{+\infty}du_0 e^{\frac{M_K}{2}(u_0+v_0)}\\ &\qquad\left\langle 0\left|T\left\{(\varepsilon_1)_\mu J_\mu(\vec{u},u_0)(\varepsilon_2)_\nu J_\nu(\vec{v},v_0)\mathcal{H}_W(0)\right\}\right|K_L(\vec{p}_K=\vec{0})\right\rangle_{\text{sub}}.\end{aligned} \tag{3}$$

Here $\pm\vec{k}$ are the momenta of the two photons with polarizations ε_1 and ε_2. Each has energy $M_K/2$ where M_K is the kaon mass. In this calculation the weak Hamiltonian density $\mathcal{H}_W$ in Eq. (1) contains the leading current-current operators Q_1 and Q_2. Note we have broken the symmetry between the two electromagnetic currents by assuming $u_0 \geq v_0$. The "sub" label on the matrix element appearing Eq. (3) indicates that subtractions which are discussed below have been performed.

While the Euclidean-space correlation function that appears in Eq. (3) contains the on-shell decay amplitude for $K_L \to \gamma\gamma$, it is complicated by the now-familiar possible contributions from additional unphysical processes in which intermediate states with energies below that of the kaon appear. For example, when applied to the kaon state $\mathcal{H}_W$ can create a neutral pion which can then couple to the two final photons. Regulating the time integrals in Eq. (3) by introducing a finite upper limit T on the v_0 integral and the same upper limit on the time separation $u_0 - v_0$, the π^0 contribution can written

$$\begin{aligned}\mathcal{A}^{\pi^0}_{\mu\nu}(\vec{u},\vec{v}) &= \int_0^T dv_0\int_{v_0}^{T+v_0}du_0\, e^{\frac{M_K}{2}(u_0+v_0)}\\ &\qquad\left\langle 0\left|J_\mu(\vec{u},u_0)J_\nu(\vec{v},v_0)\right|\pi^0\right\rangle\left\langle\pi^0\left|\mathcal{H}_W(0)\right|K_L\right\rangle \qquad (4)\\ &= \left[\frac{e^{(M_K-M_\pi)T}-1}{M_K-M_\pi}\right]\int_0^T dw_0 e^{\frac{M_K}{2}w_0}\\ &\qquad\left\langle 0\left|J_\mu(\vec{u},w_0)J_\nu(\vec{v},0)\right|\pi^0\right\rangle\left\langle\pi^0\left|\mathcal{H}_W(0)\right|K_L\right\rangle \qquad (5)\end{aligned}$$

where to obtain Eq. (5) from Eq. (4) we have changed variables from u_0 to $w_0 = u_0 - v_0$ and used the known energy of the $|\pi^0\rangle$ state to perform the integral over v_0. For this π^0 example the "-1" term inside the square bracket in Eq. (5) is the physical contribution of the π^0 intermediate state to the $K_L \to \gamma\gamma$ decay amplitude while the term that grows exponentially with increasing T is not of physical interest and must be removed from the Euclidean expression.

Of the possible intermediate states with energy less than M_K that should be considered, the vacuum and two-pion state do not appear because we are studying the decay of a K_L and neglecting the small CP violating contribution. Likewise the $\pi\pi\gamma$ intermediate state shown in Fig. 2(b) must have an energy above M_K because the two pions are not at rest but carry the momentum of the photon with a magnitude $M_K/2$ which implies $E_{\pi\pi\gamma} \geq 2\sqrt{(M_K/4)^2 + M_\pi^2} + M_K/2 = 616\text{MeV} > M_K$. While this inequality implies that for large T the unphysical term coming from the $\pi\pi\gamma$ intermediate state will vanish, the size of its actual contribution should be investigated carefully. For our present study this term will be ignored.

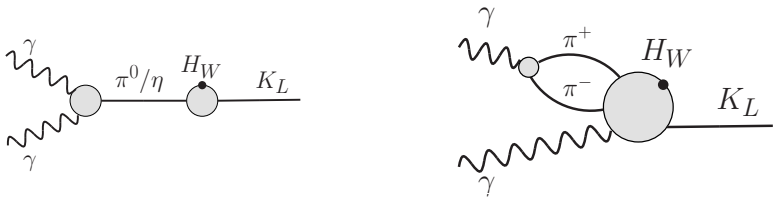

Figure 2: Schematic representations of three possible intermediate states which may have lower energy than that of the kaon and contribute unphysical terms which grow exponentially in the difference between the time when the two final-state photons are absorbed and the time at which the weak operator $\mathcal{H}_W$ is inserted.

Of greater immediate concern are the π^0 and η intermediate states shown in Fig. 2(a). The π^0 intermediate state dominates the Euclidean correlation function being studied but, as in the calculation of ΔM_K, its unphysical contribution can be accurately computed and subtracted. The η state is more difficult. While $M_\eta > M_K$ their difference is not large making the exponential fall-off of the unwanted term slow and the $M_K - M_\eta$ energy denominator, similar to the $M_K - M_\pi$ in Eq. (4), also small. Since disconnected diagrams play a large role in this $K_L - \eta$ amplitude, this term also has a large statistical uncertainty and we expect that it is best to add an extra $c_s(\bar{s}d + \bar{d}s)$ term to $\mathcal{H}_W$ with the coefficient c_s adjusted to make the matrix element $\langle\eta|\mathcal{H}_W|K_L\rangle = 0$. This was the most effective strategy for dealing with the η intermediate state in the calculation of ΔM_K [6].

3. Computational strategy

We begin by using Eq. (3) to express the K_L decay amplitude into the single $J = 0$, parity odd, two-photon final state in terms of a Euclidean correlation function depending three time coordinates:

$$\widetilde{\mathcal{A}}(v_0, x_0, t_K) = \int d^3u d^3v \int_{v_0}^{\infty} du_0 E_{\mu\nu}(u, v) \left\langle J_\mu(\vec{u}, u_0) J_\nu(\vec{v}, v_0) \mathcal{H}_W(\vec{x}, x_0) K_L(t_K) \right\rangle_{\text{sub}}. \quad (6)$$

Here $E_{\mu\nu}$ is a known function determined by the two-photon final-state and $K_L(t_K)$ is an interpolating operator which creates a zero-momentum K_L meson localized at the time t_K. Spatial

translational symmetry implies that the right-hand side does not depend spatial position $\vec{x}$ of the weak Hamiltonian density $\mathcal{H}_W$. To extract the $K_L \to \gamma\gamma$ decay amplitude we must evaluate Eq. (6) at large positive values of $x_0 - t_K$ and identify the coefficient of the $\exp[-M_K(x_0 - t_K)]$ term.

Although we must ultimately sum over the earliest time coordinate v_0 appearing in the product of the electromagnetic currents, it is important to begin by obtaining this correlation function for each value of $v_0 - x_0$. This will allow us to identify the exponentially increasing contribution of the π^0 intermediate state and demonstrate that this contribution has been removed when the independently computed π^0 contribution has been subtracted. Such a careful study of the $v_0 - x_0$ dependence will also be important in the next stage of this work in which the disconnected diagrams are evaluated and the contribution of the η intermediate state must also be removed.

While the four-point correlation function in Eq. (6) is to be evaluated in infinite volume, once the π^0 intermediate state has been removed, this hadronic amplitude is exponentially localized and can be computed in lattice QCD in a finite volume with finite-volume errors which decrease exponentially in the spatial and temporal size of the lattice volume. Thus, we can compute the $K_L \to \gamma\gamma$ decay amplitude using lattice QCD by evaluating the Euclidean four-point correlation shown in Eq. (6), perhaps summed over $\vec{x}$ to increase statistics, in the limit of large $x_0 - t_K$. We will now describe the strategies used to compute the five quark-line topologies which appear in our evaluation.

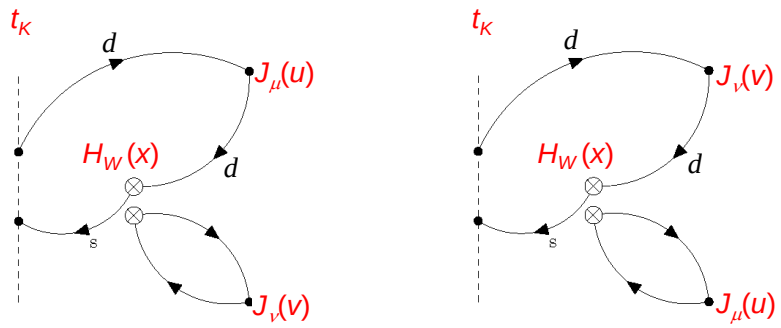

Figure 3: Two of the four quark line topologies which we label as types Ia - Id. The types Ic and Id that are not shown can be obtained from Ia and Ib by exchanging the s and d quarks. The location of the K_L interpolating operator is indicated by the vertical dotted line while the vertices corresponding to the other three operators that enter Eq. (6) are labeled explicitly.

Figure 3 shows two of the four quark-line contractions which we identify as types I(a), I(b), I(c) and I(d). In our calculation the K_L interpolating operator is constructed from a Coulomb-gauge wall source that is used to obtain twelve strange and twelve light quark propagators, one for each spin and color. For this type I topology three of the quark lines which join to the weak operator vertex correspond to point-source propagators with their source at x. These point sources are randomly distributed over the spatial volume at the time x_0. For explicit calculation described below 500 such point source propagators are computed for each configuration, distributed randomly over the entire space-time volume.

In order to evaluate the contribution of the correlation functions shown in Fig. 3 to the $K_L \to \gamma\gamma$

decay amplitude we must multiply these hadronic correlation functions by the electromagnetic factor $E_{\mu\nu}(u,v)$ and sum over the spatial coordinates $\vec{u}$ and $\vec{v}$. For these type I topologies this could require a computationally expensive V^2 operations where V is the spatial volume. This computational cost can be reduced to one of order $V \ln V$ by exploiting the translational symmetry of $E_{\mu\nu}(u,v)$ and using the convolution theorem:

$$\sum_{\vec{v},u} F(u)G(\vec{v},v_0)E(u-v) = \sum_{\vec{v}} G(\vec{v},v_0)\left\{\sum_{u} F(u)E(u-v)\right\} \tag{7}$$

$$= \sqrt{VT'}\sum_{\vec{v}} G(\vec{v},v_0)\left[\widetilde{F(-k)\widetilde{E}(k)}\right](v). \tag{8}$$

where the components k_μ of the vector k are proportional to integers n_μ with $k_i = 2\pi n_i/L$ and $-L/2 < n_i < L/2$ for an even lattice size L and $1 \le i \le 3$ while $k_0 = 2\pi n_0/T'$ with $-T'/2 < n_0 \le T'/2$. Here T' is the number of sites over which u_0 is summed, which is 32 in the calculation presented here. The tilde indicates Fourier transformation, for example:

$$\widetilde{F}(k) = \sum_{u} \frac{e^{-iku}}{\sqrt{VT'}} F(u). \tag{9}$$

Here the functions $F(u)$ and $G(v)$ represent the separate factors in terms of which the correlation functions of type I can be expressed. This factorization requires that the contractions performed with the weak operator be treated as a sum of terms which are each evaluated using this convolution strategy.

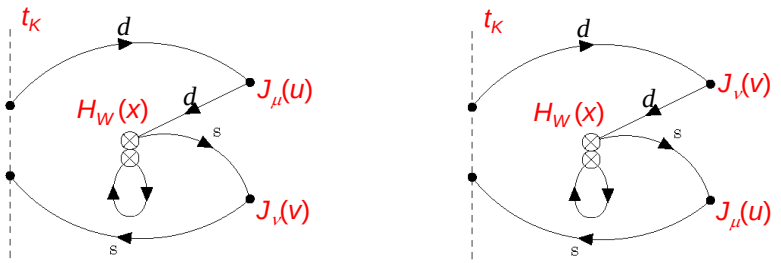

IIa IIb

Figure 4: Two of the four quark line topologies which we label as types IIa - IId. The types IIc and IId that are not shown can be obtained from IIa and IIb by exchanging the s and d quarks.

Two of the four type II topologies are shown in Fig. 4. These are evaluated using the same convolution strategy as was employed for type I. As is the case for type I, three point-source propagators are needed with the point source located at the position of the weak operator. For the case of type II, one of those point-source propagators is evaluated at the location of the weak operator forming the closed loop.

Figure 5 shows the single type III topology. For this case we use two point-source propagators whose source is at the location v of the current evaluated at the earliest time, one of the three times identified in the amplitude being computed as shown in Eq. (6). The point source propagator

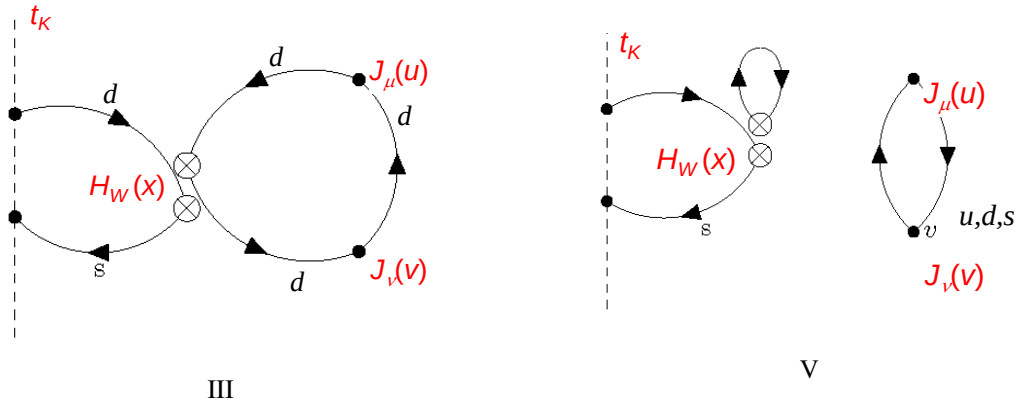

Figure 5: Diagrams showing the quark line topologies which we label as types III and V.

connecting the positions u with v in Fig. 5 is then multiplied by the electromagnetic factor $E_{\mu\nu}(u,v)$ and the product, viewed as a function of u, is used as a source for a second solution to the Dirac equation. The resulting "sequential" propagator is then evaluated at the location x of the weak operator and the result, when combined with the second point source propagator evaluated at x summed over all values of $\vec{x}$ and the results saved for each value of the time x_0. As for types I and II, in the calculation presented here we use 500 point source propagators with point sources randomly distributed over the space-time volume.

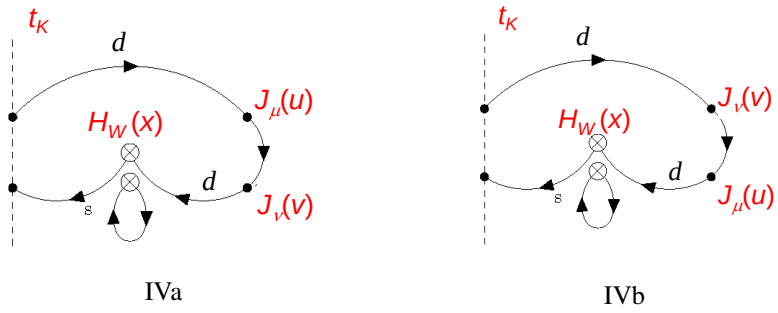

Figure 6: Two of the four quark line topologies which we label as types IVa - IVd. The types IVc and IVd that are not shown can be obtained from IVa and IVb by exchanging the s and d quarks.

Two of the four type IV diagrams are shown in Fig. 6. These are evaluated by using two point-source propagators with source at the position v. The loop propagator with source and sink at the location of the weak operator is evaluated using an all-to-all propagator. For the calculation described here we construct these all-to-all propagators from the 2,000 Dirac eigenvectors with the smallest eigenvalues and then use propagators constructed from 768 sources, each distributed stochastically over the full space-time volume but each source with a specific spin and color, to correct for the difference between the low-mode approximation to this propagator and the exact inverse of the Dirac operator. For the explicit calculation described below these 2,000 eigenvectors where computed using a different variant of the domain wall fermion Dirac operator than used in the rest of the calculation. While this introduces no bias in the resulting all-to-all propagators, this imperfection in the low modes that were used increases the size of the stochastic correction and the

correspond noise it introduces.

The type V diagrams are shown in Fig. 5. This class of disconnected graphs has been evaluated but are not included in the results discussed below. There are other disconnected graphs in which one or both of the current operators appears in a disconnected loop. These diagrams are expected to be small because they vanish in the limit in which the three flavors of quarks have the same mass and because they must be connected to the other parts of the diagram by at least three gluon propagators.

These type V diagrams are evaluated by using an all-to-all propagator for the closed loop that is joined to the weak vertex shown in the right panel of Fig. 5 and a point-source propagator with source at the location v. This will allow a sum over all spatial positions $\vec{x}$ of the weak operator and all space time locations u for the second current with $u_0 \geq u_0$.

4. Initial results

We have applied the strategies described above in an exploratory calculation performed on 117 gauge configurations separated by 10 molecular dynamics time units taken from an ensemble generated with 2+1 flavors of Mobius domain wall fermions, a lattice volume of $24^3 \times 64$, an inverse lattice spacing $1/a = 0.98(4)$ GeV and physical light and strange quark masses. The gauge action is a combination of the Iwasaki gauge action and the dislocation suppressing determinant ratio (DSDR). We show results from diagrams of type I through IV. These are all connected graphs and results from disconnected graphs are not included. The calculation was performed with the kaon wall source located alternately at each of the 64 possible values of t_K for each configuration and the results averaged.

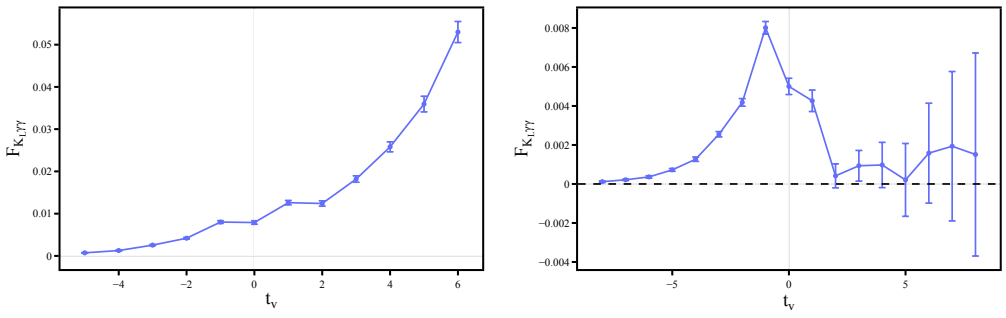

(a) (b)

Figure 7: Plots of the amplitude shown in Eq. (3) as a function of $t_v = v_0 - x_0$. (a) The left panel shows the result including the pion intermediate state. (b) The right panel shows the amplitude after the contribution of the pion intermediate state has been removed.

In Fig. 7(a) we show the result from the sum of these four types of diagram before the contribution from the intermediate pion state has been subtracted as a function of $t_v = v_0 - x_0$. The expected exponential growth with increasing t_v is seen with an exponent matching the expected $(M_K - m_\pi)t_v$ within errors. Figure 7(b) shows the same quantity after the contribution of the π^0 intermediate state has been removed. Here the exponentially growing π^0 contribution which

is subtracted is obtained from separate calculations of the $\langle 0|J_\mu J_\nu|\pi^0>$ and $\langle \pi^0|H_W|K_L\rangle$ matrix elements which appear in Eq. (5). The accurate cancellation seen in Fig. 7(b) provides a consistency check on the calculation.

We should point out an important subtlety that arises when working only with the connected graphs. In this case there are two neutral mesons with the mass of the pion: the usual $I = 1$, $I_z = 0$, π^0 meson and a second degenerate $I = 0$ pion. This second unphysical state should combine with the omitted disconnected contributions to form the physical η state. However, in our present circumstances both states are present and both must be subtracted to obtain a "physical" connected result.

The final result for the decay form factor $F_{K_L\gamma\gamma}$ from the connected diagrams can be obtained by computing the area under the curve shown in Fig. 7(b) and adding to it the π^0 contribution arising from the "-1" term in the square brackets in Eq. (5). This is the physical contribution of the π^0 intermediate state that was incorrectly removed when we subtracted the entire π^0 contribution when obtaining the result plotted in Fig. 7(b). The preliminary result for the connected contribution to the form factor is

$$F_{K_L\gamma\gamma} = 0.0129(27). \tag{10}$$

The error is statistical only and the result is somewhat smaller than the experimental value $F_{K_L\gamma\gamma} = 0.02047(9)$.

5. Outlook

The initial results described above are incomplete because the contribution of the disconnected diagrams has not been included. While we have computed what we expect to be the leading disconnected diagram, the type V diagram shown in Fig. 5, the results have large statistical errors. Because of the near degeneracy of the kaon and η mesons, as discussed above, we must remove the η intermediate state by adding an $\bar{s}d + \bar{d}s$ term to H_W, an added complication made more difficult by the large statistical noise. It is possible that a much more extensive calculation will be needed to determine the disconnected contribution. We may need to add far more gauge configurations to the current calculation or to work at a much smaller lattice spacing, as has been done in the calculation of ΔM_K where meaningful results for the disconnected diagrams have been obtained [6]. Thus, continued study of this $K_L \to \gamma\gamma$ process is warranted.

Our goal of computing the two-photon contribution to the strangeness-changing, neutral-current process $K_L \to \mu^+\mu^-$ will also require that the statistical noise present in the disconnected parts be controlled. However, it will also be necessary to develop additional techniques to treat the $\pi\pi\gamma$ intermediate state. While in the $K_L \to \gamma\gamma$ case the two-pion state must carry the momentum of one of the photons, this is no longer true for the two-muon decay and the effects of this three-particle state must be understood. These effects include both the unphysical exponentially growing terms that arise because the energy of the $\pi\pi\gamma$ can be less than M_K and the potentially large finite-volume errors that can arise from kinematics where the $\pi\pi\gamma$ has an energy close to M_K. Treating this second effect will require a generalization of the two-particle analysis given in Ref. [7]. Thus, considerable further effort will be needed before the two-photon contribution to $K_L \to \mu^+\mu^-$ can be computed.

Acknowledgement

This work supported by US DOE grant #DE-SC0011941. The authors thank Luchang Jin for providing the point- and wall-source propagators, Tom Blum and Dan Hoying for the 2000 Dirac low modes for each configuration, Ryan Abbott for the non-perturbative renormalization factors for the weak operators Q_1 and Q_2, Chris Kelly for the code used to generate the all-to-all propagators and Peter Boyle for the Grid framework in which the code was written. This research used resources of the National Energy Research Scientific Computing Center (NERSC), a U.S. Department of Energy Office of Science User Facility located at Lawrence Berkeley National Laboratory, operated under Contract No. DE-AC02-05CH11231 using NERSC award HEP-ERCAP13527.

References

[1] Particle Data Group collaboration, P. A. Zyla et al., *Review of Particle Physics*, *PTEP* **2020** (2020) 083C01.

[2] T. Blum, N. Christ, M. Hayakawa, T. Izubuchi, L. Jin and C. Lehner, *Lattice Calculation of Hadronic Light-by-Light Contribution to the Muon Anomalous Magnetic Moment*, *Phys. Rev. D* **93** (2016) 014503 [1510.07100].

[3] J. Green, N. Asmussen, O. Gryniuk, G. von Hippel, H. B. Meyer, A. Nyffeler et al., *Direct calculation of hadronic light-by-light scattering*, *PoS* **LATTICE2015** (2016) 109 [1510.08384].

[4] N. H. Christ, X. Feng, L. Jin, C. Tu and Y. Zhao, *Lattice QCD calculation of the two-photon contributions to $K_L \to \mu^+\mu^-$ and $\pi^0 \to e^+e^-$ decays*, *PoS* **LATTICE2019** (2020) 128.

[5] N. H. Christ, X. Feng, L. Jin, C. Tu and Y. Zhao, *Calculating the Two-photon Contribution to $\pi^0 \to e^+e^-$ Decay Amplitude*, *PoS* **LATTICE2019** (2020) 097 [2001.05642].

[6] B. Wang, *Calculation of the $K_L - K_S$ mass difference for physical quark masses*, *PoS* **LATTICE2019** (2019) 093 [2001.06374].

[7] N. H. Christ, X. Feng, G. Martinelli and C. T. Sachrajda, *Effects of finite volume on the K_L-K_S mass difference*, *Phys. Rev. D* **91** (2015) 114510 [1504.01170].